Hydrodynamics of Turning Flocks

Xingbo Yang[1,*] and M. Cristina Marchetti[1,2]
[1]Physics Department, Syracuse University, Syracuse, New York 13244, USA
[2]Syracuse Biomaterials Institute, Syracuse University, Syracuse, New York 13244, USA
(Received 21 October 2014; revised manuscript received 7 August 2015; published 17 December 2015)

We present a hydrodynamic model of flocking that generalizes the familiar Toner-Tu equations to incorporate turning inertia of well-polarized flocks. The continuum equations controlled by only two dimensionless parameters, orientational inertia and alignment strength, are derived by coarse-graining the inertial spin model recently proposed by Cavagna *et al.* The interplay between orientational inertia and bend elasticity of the flock yields anisotropic spin waves that mediate the propagation of turning information throughout the flock. The coupling between spin-current density to the local vorticity field through a nonlinear friction gives rise to a hydrodynamic mode with angular-dependent propagation speed at long wavelengths. This mode becomes unstable as a result of the growth of bend and splay deformations augmented by the spin wave, signaling the transition to complex spatiotemporal patterns of continuously turning and swirling flocks.

DOI: 10.1103/PhysRevLett.115.258101 PACS numbers: 87.23.Cc, 05.65.+b, 47.54.-r, 87.18.Hf

The Vicsek model [1,2] and related continuous-time variations [3] have been used to model flocking in a variety of systems, including birds [4] and cells [5] as well as *in vitro* cellular components [6,7] and synthetic swimmers [8]. These are examples of active systems, consisting of individually driven, dissipative units that exhibit coordinated motion (flocking) at large scales [9,10]. In the Vicsek model the active units are described as point particles with overdamped dynamics carrying a velocity vector of fixed magnitude, and are hence called "flying spins." Each spin tends to align with its neighbors, but the spins do make errors, which are modeled as angular noise [2]. The system exhibits a liquid-gas phase transition from a disordered gas state to a polar liquid state as the noise is decreased or the number density is increased, with microphase separation in the coexistence region [11]. The existence of the transition has been set on firm grounds by a large number of numerical studies [2,12]. Toner and Tu also proposed a continuum version of the model, inspired by dynamical field theories of condensed-matter systems [13,14].

Recent work [15] has suggested that the description of the observed collective turning of bird flocks requires a modification of the Vicsek model to include angular inertia in the dynamics. This allows for the propagation of angular correlations through the flock on large scales via spin-wave-like excitations [16]. In this Letter we derive the continuum equations for such an "inertial spin model" by explicitly coarse-graining the microscopic dynamics. The resulting equations [Eqs. (6)–(8)] generalize the Toner-Tu model to account for turning modes by incorporating the dynamics of the spin angular momentum of the flock. These equations, governed by only two dimensionless parameters, are the first important result of our Letter. They contain new terms as compared to the phenomenological model of Ref. [17], the most important being a nonlinear friction that couples spin and density fluctuations to bend and splay deformations of the order parameter. This new coupling transforms the propagating density bands ubiquitously observed in flocking models into turning bands of spin currents, driving the transition to a novel state of continuously swirling and rotating flocks, where turning information is transmitted by anisotropic propagating spin waves. The predicted sound speeds could in principle be measured in experiments.

Our starting point is the continuous-time model of inertial spins proposed by Cavagna *et al.* [16], where N point particles in a two-dimensional box of area L^2, with average number density $\rho_0 = N/L^2$, interact via a pairwise aligning interaction. Each particle is described by its position $\boldsymbol{r}_i$ and the direction of its velocity, identified by a unit vector $\hat{\boldsymbol{e}}_{\theta_i} = (\cos\theta_i, \sin\theta_i)$ in 2D. The dynamics of the ith spin is described by

$$\frac{d\boldsymbol{r}_i}{dt} = v_0\hat{\boldsymbol{e}}_{\theta_i}, \qquad \frac{d\theta_i}{dt} = \frac{1}{\chi}s_i, \tag{1}$$

$$\frac{ds_i}{dt} = \gamma\sum_j \tilde{F}(\theta_j - \theta_i, \boldsymbol{r}_{ji}) - \frac{\eta}{\chi}s_i + \sqrt{2\epsilon}\xi_i(t), \tag{2}$$

with $\boldsymbol{r}_{ji} = \boldsymbol{r}_j - \boldsymbol{r}_i$, v_0 the self-propulsion speed, s_i the spin angular momentum, and χ the spin moment of inertia. The spin is an internal angular momentum that generates the self-rotation, and is distinct from the angular momentum of the center of mass. The polar aligning interaction of strength γ is given by $\tilde{F}(\theta, \boldsymbol{r}) = \sin(\theta)/(\pi R^2)$ if $|\boldsymbol{r}| \le R$ and zero otherwise, with R the range of interaction. This form of the interaction, used before in the literature [18], allows us to make analytical progress in the derivation of

the continuum equations. Finally, η is a friction and ϵ describes the strength of the angular noise, with $\xi_i(t)$ a Gaussian white noise with zero mean and unit variance.

On time scales large compared to the relaxation time $\tau_\eta = \chi/\eta$, one can neglect the time derivative on the left-hand side of Eq. (2) and eliminate the spin angular momentum, s_i, from the angular dynamics. This yields a continuous-time version of the Vicsek model, with effective alignment strength γ/η and effective angular noise ϵ/η^2. Two additional time scales govern the dynamics of the system: the effective rotational diffusion time, $\tau_\epsilon = \eta^2/\epsilon$, and the alignment time, $\tau_\gamma = \eta/(\gamma\rho_0)$.

Following standard methods [19,20], one obtains the noise-averaged Fokker-Planck equation associated with the microscopic dynamics described by Eqs. (1) and (2), as

$$\left(\mathcal{D}_t + \frac{s}{\chi}\partial_\theta\right)P = \partial_s\left[\left(\eta\frac{s}{\chi} + T[P]\right)P\right] + \epsilon\partial_s^2 P, \tag{3}$$

where $\mathcal{D}_t = \partial_t + v_0\boldsymbol{e}_\theta\cdot\boldsymbol{\nabla}$ is the material derivative, $P(\boldsymbol{r},\theta,s,t)$ is the probability density of particles at position $\boldsymbol{r}$, with velocity in direction θ and spin s at time t, and $T[P]$ is the aligning torque

$$T[P] = -\gamma\int_{\theta'}\int_{s'} F(\theta'-\theta)P(\boldsymbol{r},\theta',s',t). \tag{4}$$

For simplicity we have assumed $\tilde{F}(\theta,\boldsymbol{r}) = \delta(\boldsymbol{r})F(\theta)$, with $F(\theta) = \sin(\theta)$, neglecting interaction between pairs at different positions.

We describe the large-scale dynamics in terms of a few coarse-grained fields that vary slowly relative to microscopic time scales. For polarized flocks, in addition to the number density, $\rho(\boldsymbol{r},t)$, of active units and their polarization-current density, $\boldsymbol{w}(\boldsymbol{r},t)$, we include the spin-angular-momentum density, $S(\boldsymbol{r},t)$. These are obtained from the probability density P as

$$\begin{pmatrix}\rho(\boldsymbol{r},t)\\ \boldsymbol{w}(\boldsymbol{r},t)\\ S(\boldsymbol{r},t)\end{pmatrix} = \int_\theta\int_s\begin{pmatrix}1\\ \hat{\boldsymbol{e}}_\theta\\ s\end{pmatrix}P(\boldsymbol{r},\theta,s,t). \tag{5}$$

To obtain a closed set of hydrodynamic equations for ρ, $\boldsymbol{w}$, and $\boldsymbol{S} = S\hat{\boldsymbol{z}}$, we combine moment techniques used to approximate the velocity-dependent part of the Fokker-Planck equation [21] with the closure developed in Refs. [22,23] to handle kinetic equations of active systems (see Supplemental Material [24]). To minimize the number of parameters, we nondimensionalize the equations by scaling time with $\tau_\epsilon = \eta^2/\epsilon$, length with $v_0\tau_\epsilon$, and density with $\rho_0 = N/L^2$. The resulting equations are controlled by only two dimensionless parameters, $\tilde{\chi} = \tau_\eta/\tau_\epsilon$ and $\tilde{\gamma} = \tau_\epsilon/\tau_\gamma$ [24]. For simplicity, we drop the tildes and all parameters are dimensionless in the following discussion unless otherwise noted. The continuum equations are given by

$$\frac{\partial\rho}{\partial t} = -\boldsymbol{\nabla}\cdot\boldsymbol{w}, \tag{6}$$

$$\mathcal{D}_t^w\boldsymbol{w} = -[\alpha(\rho)+\beta|\boldsymbol{w}|^2]\boldsymbol{w} - \frac{1}{2}\boldsymbol{\nabla}\rho + \lambda_2\boldsymbol{w}(\boldsymbol{\nabla}\cdot\boldsymbol{w}) + \Omega_1\boldsymbol{S}\times\boldsymbol{w} + \Omega_2\boldsymbol{\nabla}\times\boldsymbol{S} + D_w\nabla^2\boldsymbol{w}, \tag{7}$$

$$\mathcal{D}_t^s\boldsymbol{S} = -\boldsymbol{\nabla}\times\{[\alpha(\rho)+\beta|w|^2]\boldsymbol{w}\} + \Omega_3\boldsymbol{w}\times\nabla^2\boldsymbol{w} - \lambda_s(\boldsymbol{\nabla}\cdot\boldsymbol{w})\boldsymbol{S} - \xi\boldsymbol{S} + D_s\nabla^2\boldsymbol{S}, \tag{8}$$

where $\mathcal{D}_t^w = \partial_t + \lambda_1\boldsymbol{w}\cdot\boldsymbol{\nabla}$ and $\mathcal{D}_t^s = \partial_t + \lambda_s\boldsymbol{w}\cdot\boldsymbol{\nabla}$ are convective derivatives, $\alpha(\rho) = (1-\gamma\rho/2)/(1+\chi)$, $\beta = \gamma^2/[8(1+\chi)]$, and $\xi = 1/\chi$. Explicit expressions for all other dimensionless parameters are given in the Supplemental Material [24]. A pressure-type term $\lambda_3\nabla|w|^2$ has been neglected in Eq. (7) because this term is known to lead to a spurious instability, even in the overdamped limit when λ_3 is evaluated with the closure used here [23,25]. This instability has not been observed in particle simulations of Vicsek models. We have also verified that it is not obtained in particle simulations of the inertial spin model.

Equations (6)–(8) augment the flocking model of Toner and Tu [13] by incorporating the dynamics of the spin current. When $\boldsymbol{S}$ is neglected, these equations reduce to the Toner-Tu equations as derived by Farrell *et al.* [18] (but for the case of constant self-propulsion speed). As in the Toner-Tu model, the vector field $\boldsymbol{w}$ plays the dual role of polarization density and flow velocity. In equilibrium systems of rotors, both the equations for the spin and the velocity field $v_0\boldsymbol{w}$ would contain dissipative couplings describing friction with the substrate proportional to the combination $\boldsymbol{S}/\chi - (v_0/2)\boldsymbol{\nabla}\times\boldsymbol{w}$, guaranteeing that the angular velocity $\boldsymbol{S}/\chi$ and the vorticity $(v_0/2)\boldsymbol{\nabla}\times\boldsymbol{w}$ be equal when the whole system is rotating as a rigid body [26,27]. In the nonequilibrium system considered here, in contrast, frictional terms proportional to angular velocity and vorticity will, in general, appear with different coefficients. The first term on the right-hand side of Eq. (8) was not included in previous phenomenological model [17] and has a natural interpretation of a nonlinear, velocity-dependent vortical friction. The "self-spinning" term $\boldsymbol{S}\times\boldsymbol{w}$ couples the center-of-mass motion to the turning dynamics. In contrast to systems of passive rotors [26,28], in the self-propelled particle model considered here, these two degrees of freedom are coupled because the spinning angle also controls the direction of translational motion [16]. We expect these equations will prove useful to describe a number of active systems where collective turning controls the large-scale dynamics.

The homogeneous steady states of the continuum equations have uniform density, $\rho = 1$, and zero mean value of the spin, $\boldsymbol{S} = 0$. As in the Toner-Tu model with no angular

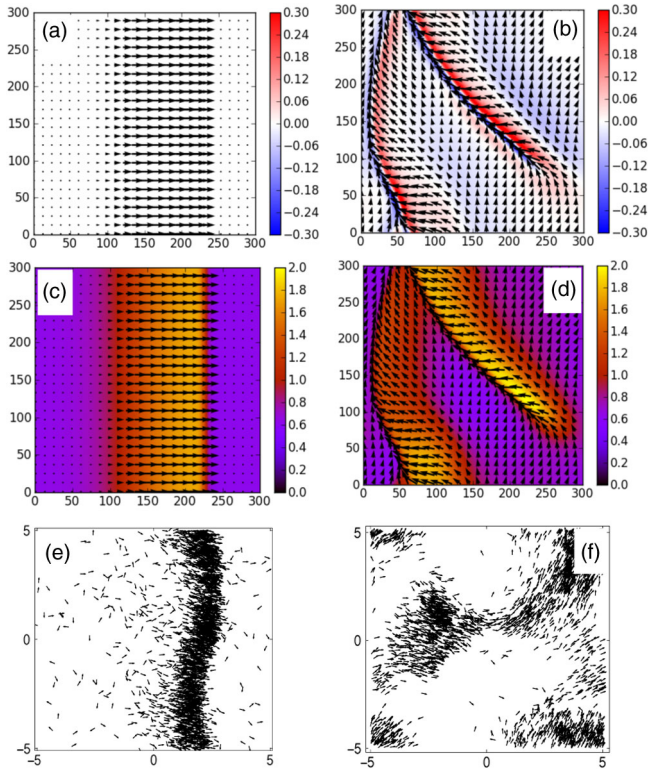

FIG. 1 (color online). Flocking patterns obtained via numerical solutions of Eqs. (6)–(8) (top and middle rows) and via particle simulations using Eqs. (1)–(2) (bottom row). The left (right) column shows the patterns obtained at points A (B) of the phase diagram Fig. 2(a), corresponding to the spinodal portion of the coexistence region of traveling bands of polar liquid and disordered gas and to the region of the spin-wave instability, respectively. The snapshots (a)–(d) are obtained with $\tilde{\gamma} = 2.0$, $\tilde{\chi} = 0.5$ [(a),(c)] and $\tilde{\gamma} = 7.6$, $\tilde{\chi} = 1.7$ [(b),(d)] on a 300×300 grid lattice with grid size 0.1, integration time step 0.002, and periodic boundary conditions. The particle simulations are performed with 3000 particles in a box of size $L = 10$ with periodic boundary conditions. Simulation parameters are $R = 1$, $\epsilon = 2.0$, $v_0 = 2.0$, $\chi = 1.0$, $\eta = 1.0$, and $\gamma = 0.16$ (e) or $\gamma = 0.80$ (f). The integration time step is 0.01. In (a)–(d), the arrows represent the local polarization, with length proportional to the polarization strength. The color indicates spin-current density in (a)–(b) and number density in (c)–(d). In (e)–(f), the arrows represent polarization of individual particles (see movies in Supplemental Material [24]).

inertia, there are two such states: an isotropic gas state, with $\boldsymbol{w} = 0$, and a polarized liquid or flocking state, with $\boldsymbol{w} = w_0\hat{\boldsymbol{x}}$ and $w_0 = \sqrt{-\alpha_0/\beta}$, where $\alpha_0 = \alpha(\rho = 1)$. We have chosen the $\hat{\boldsymbol{x}}$ axis along the direction of spontaneously broken symmetry. The isotropic state is always linearly stable for $\gamma < 2$. We examine below the linear stability of the polarized state by considering the dynamics of fluctuations. We let $\boldsymbol{w} = w_0\hat{\boldsymbol{x}} + \delta\boldsymbol{w}$, $\rho = 1 + \delta\rho$, $\boldsymbol{S} = \hat{\boldsymbol{z}}\delta s$, and introduce Fourier amplitudes $(\delta\rho, \delta\boldsymbol{w}, \delta s) = \sum_{\boldsymbol{q}}(\rho_{\boldsymbol{q}}, \boldsymbol{w}_{\boldsymbol{q}}, s_{\boldsymbol{q}})e^{i\boldsymbol{q}\cdot\boldsymbol{r}+\sigma t}$ to obtain a set of linearized equations in Fourier space (see Supplemental Material [24]).

For spatial variations along the direction of broken symmetry ($\boldsymbol{q} = q\hat{\boldsymbol{x}}$), $w_{\boldsymbol{q}}^y$ and $s_{\boldsymbol{q}}$ decouple from $\rho_{\boldsymbol{q}}$ and $w_{\boldsymbol{q}}^x$. The coupled linear dynamics of fluctuations in the density and the magnitude of polarization ($w_{\boldsymbol{q}}^x$) is unaffected by angular inertia and is controlled by a longitudinal propagating mode, with propagation speed $c_\rho = |\alpha_\rho|/(2\beta w_0)$, where $\alpha_\rho = \partial_\rho\alpha$. This mode goes unstable when $\gamma < 8/3$, corresponding to region A in Fig. 2(a). This instability is known in the Vicsek and Toner-Tu models as banding instability, but has recently been identified as the spinodal boundary within the liquid-gas coexistence region (Fig. 1, left column) [11,22,25,29]. The coupled dynamics of spin and bending fluctuations ($w_{\boldsymbol{q}}^y$) gives rise to overdamped, finite-wavelength spin waves that mediate the propagation of turning information throughout the flock with wave speed $c_s = w_0\sqrt{\Omega_1\Omega_3}$ that increases with alignment strength. The existence of such propagating spin waves has been demonstrated on the basis of general arguments [16] and phenomenological continuum models [17], where they were dubbed "second sound."

For wave vectors along any direction other than that of broken symmetry, all four equations are coupled and the analysis of the modes is rather cumbersome. For small wave vectors, we find two stable and relaxational modes (which will not be discussed further) and two hydrodynamic propagating modes, with dispersion relation

$$\sigma^{\pm}(q,\theta) = ic^{\pm}(\theta)q - \mathcal{D}_{sw}(\theta)q^2 + \mathcal{O}(q^3) \qquad (9)$$

and wave velocity

$$c^{\pm}(\theta) = \frac{\alpha_\rho\cos(\theta) \pm \sqrt{\alpha_\rho^2\cos^2(\theta) + 8\beta^2 w_0^2\sin^2(\theta)}}{4\beta w_0}, \qquad (10)$$

where θ is the angle between the direction of $\mathbf{q}$ and the direction of broken symmetry. The full expression for the damping $\mathcal{D}_{sw}(\theta)$ is not instructive and, thus, is not given here. For $\theta = 0$, $c^-(0) = \alpha_\rho/(2\beta w_0)$ and the mode σ^- yields the banding instability that delimits the spinodal region of microphase separation [11]. For arbitrary angle θ, however, both modes propagate with anisotropic speed and describe coupled fluctuations of density, spin, and bend or splay deformations of the polarization field. The angular dependence of the instability is shown in Fig. 2(b), which displays the regions where $\mathcal{D}_{sw} < 0$. At small angles, the instability is driven by density fluctuations, as in the Toner-Tu model. At large angles, the instability is dominated by spin fluctuations. At $\theta = \pi/2$, the longitudinal banding instability is suppressed and the dynamics is controlled by the transverse spin wave propagating at speed $|c^{\pm}(\pi/2)| = 1/\sqrt{2}$. In terms of our dimensionless parameters, this transverse spin wave is unstable for $\gamma > (1 + 4\chi)(1 + \chi)/(8\chi^2) + 4$, corresponding to region B in Fig. 2(a). The instability is driven by the growth of bend $-\boldsymbol{\nabla} \times \{[\alpha(\rho) + \beta|w|^2]\boldsymbol{w}\}$ and splay $\lambda_2\boldsymbol{w}(\boldsymbol{\nabla}\cdot\boldsymbol{w})$

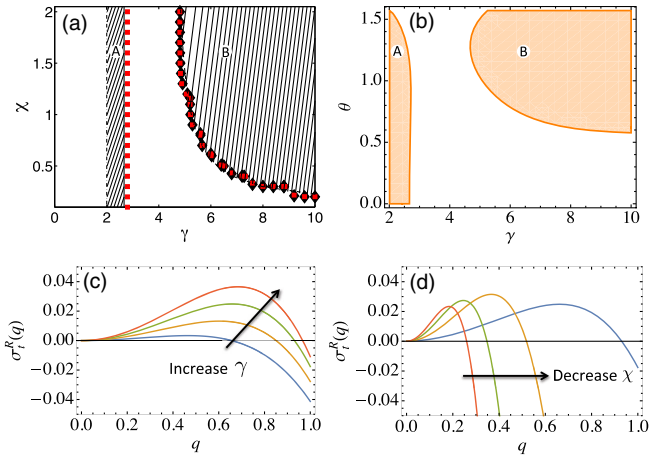

FIG. 2 (color online). (a) Phase diagram in the plane of dimensionless γ and χ. (b) Phase diagram in the plane of dimensionless γ and θ at $\chi = 1.0$. The shaded region A is the spinodal portion of the region of coexistence of disordered gas (existing for $\gamma < 2$) and traveling bands of polar liquid (existing for $\gamma > 8/3$). The coexistence region is delimited by the binodals (not shown) and extends inside the white regions, both to the right and to the left of region A, as verified via particle simulations. The shaded region B corresponds to the region where the homogeneous polar liquid is linearly unstable to spin waves, as shown in Fig. 1. (c) Real part of the dispersion relation of the transverse mode $\sigma_t^{\pm} = \sigma^{\pm}(\pi/2)$ at $\chi = 1$ and $\gamma = 7.0$, 8.0, 9.0, and 10.0. (d) Real part of the dispersion relation of the transverse mode $\sigma_t^{\pm} = \sigma^{\pm}(\pi/2)$ at $\gamma = 9$ and $\chi = 0.5$, 1.0, 1.5, and 2.0.

deformations augmented by the spin wave through the self-rotation term $\Omega_1 \boldsymbol{S} \times \boldsymbol{w}$. This long-wavelength instability of the ordered state is a new result of our Letter and will be referred to as spin-wave instability. It leads to a complex spatiotemporal dynamics with large density and spin fluctuations characterized by continuously turning and swirling flocks as confirmed by numerical solutions of the hydrodynamic equations and particle simulations (see Fig. 1, right column).

By carrying out the small wave vector expansion of the dispersion relation Eq. (9) up to fourth order in q, we can identify the wave vector q_c of the fastest-growing mode corresponding to the maximum of $\mathrm{Re}[\sigma_t^{\pm}(q)]$ shown in Figs. 2(c) and 2(d) for various values of γ and χ. This defines the characteristic length scale $\lambda_c \sim 1/q_c$, which can be thought of as controlling the size of the turning flock at the linear level.

To gain more insight on the complex spatiotemporal structures that emerge in the unstable regions of parameters and to confirm the results of the linear stability analysis, we have numerically solved Eqs. (6)–(8) with periodic boundary conditions starting from the homogeneous polar state with small perturbations. The results are summarized in the phase diagram of Fig. 2(a). The shaded region A is bounded to the left by the line $\gamma = 2$ where the disordered gas is linearly unstable and to the right by the line $\gamma = 8/3$ where the homogeneous polar liquid is linearly unstable to longitudinal fluctuations (the banding instability). These instability lines delimit the spinodal portion of the gas-liquid coexistence region and are distinct from the binodal lines that mark the boundaries of such a region [11]. In fact, particle simulations reveal that the coexistence region extends to the left and right of region A. The squares in Fig. 2(a) correspond to mean density fluctuations $\Delta\rho = \sqrt{(1/N)\sum_{\mathbf{r}}\langle[\rho(\boldsymbol{r}) - \rho_0]^2\rangle}/\rho_0 = 0.003$, with N the number of grid points, evaluated in the continuum model, starting in a uniform polar state. The shaded region B is the region where the homogenous polar liquid is linearly unstable to spin-wave fluctuations. Again, particle simulations show that the inhomogeneous spinning bands are found beyond the linear stability boundary that delimits region B, suggesting that this region is also a spinodal region. The diamonds correspond to spin fluctuations $\Delta S = \sqrt{(1/N)\sum_{\mathbf{r}}\langle[S(\boldsymbol{r}) - \langle S\rangle]^2\rangle} = 0.0003$. In the overdamped limit $\chi \to 0$, the spin-wave instability vanishes due to the rapid decay of spin-current fluctuations over time χ/η, and the dynamics of the system is controlled solely by a rescaled alignment strength γ, with a generic banding instability close to the flocking transition, as in the Vicsek and the Toner-Tu models [22,25,29]. Our result, together with Ref. [17], highlights for the first time the importance of inertia in controlling dynamics of active polar systems at large length scales.

To understand the nature of the spin waves that mediate the transfer of turning information within the flock, we study the propagation of the spin waves numerically with Eqs. (6)–(8) by initializing the system in the uniformly polarized state, with a concentrated spin current at the center [Fig. 3(a)]. We measure the longitudinal and transverse speed as a function of alignment strength γ for various χ and plot the results in Fig. 3(b). The longitudinal speed (circles) increases with the strength of

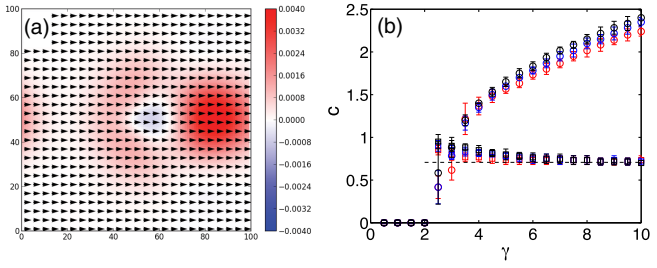

FIG. 3 (color online). (a) Snapshot of the anisotropic spin wave in the polarized state at $\gamma = 7.0$ and $\chi = 2.0$. Color indicates the spin-current density. (b) Speed of spin waves in the polarized state as a function of alignment strength γ for $\chi = 1.0$, 1.5, 2.0 (red, blue, black) in the directions longitudinal (circles) and transverse (squares) to that of mean polarization. The dashed line is the transverse speed $|c^{\pm}(\pi/2)|$ in Eq. (10). The system is evolved for 5000 time steps.

alignment interaction, while the transverse speed (squares) stays approximately constant over the range of parameters.

In the longitudinal direction, where δw_y and δs decouple from δw_x and $\delta\rho$, the spin wave is governed by a damped wave equation at finite wavelength with wave speed $c_s = w_0\sqrt{\Omega_1\Omega_3}$ proportional to alignment strength. In the transverse direction, all fluctuations are coupled and the dynamics is governed at long wavelengths by the hydrodynamic mode [Eq. (9)] with an angular-dependent propagating speed that reduces to $|c^{\pm}(\pi/2)| = 1/\sqrt{2}$ in the transverse direction as given in Eq. (10), and that fits the data quantitatively in Fig. 3(b).

We have derived continuum equations that generalize the Toner-Tu model of flocking to incorporate turning inertia by coarse-graining the active inertial spin model recently proposed by Cavagna *et al.* [16]. The coarse-graining simplifies the analysis by shrinking the number of independent parameters to two. The interplay between rotational inertia and bending elasticity of a polarized flock provides a mechanism for the propagation of turning information through the flock in the form of collective spin-wave excitations. By studying the continuum equations analytically and numerically, we predict a new instability of the polarized state associated with large density and spin-current fluctuations that leads to complex spatiotemporal patterns of continuously swirling and rotating flocks. This long-wavelength instability is associated with the growth of anisotropic spin waves and is referred to as spin-wave instability.

We thank Sriram Ramaswamy and Andrea Cavagna for useful discussions. The research leading to this work was supported by the National Science Foundation (NSF) Awards No. DMR-1305184 and No. DGE-1068780 at Syracuse University and NSF Award No. PHY11-25915 and the Gordon and Betty Moore Foundation Grant No. 2919 at the KITP at the University of California, Santa Barbara. M. C. M. also acknowledges support from the Simons Foundation.

*xyang14@syr.edu

[1] C. W. Reynolds, Computer Graphics Forum **21**, 25 (1987).
[2] T. Vicsek, A. Czirók, E. Ben-Jacob, I. Cohen, and O. Shochet, Phys. Rev. Lett. **75**, 1226 (1995).
[3] P. Romanczuk, M. Bär, W. Ebeling, B. Lindner, and L. Schimansky-Geier, Eur. Phys. J. Spec. Top. **202**, 1 (2012).
[4] M. Ballerini, N. Cabibbo, R. Candelier, A. Cavagna, E. Cisbani, I. Giardina, V. Lecomte, A. Orlandi, G. Parisi, A. Procaccini *et al.*, Proc. Natl. Acad. Sci. U.S.A. **105**, 1232 (2008).
[5] B. Szabó, G. J. Szollosi, B. Gonci, Z. Juranyi, D. Selmeczi, and T. Vicsek, Phys. Rev. E **74**, 061908 (2006).
[6] V. Schaller, C. Weber, C. Semmrich, E. Frey, and A. R. Bausch, Nature (London) **467**, 73 (2010).
[7] Y. Sumino, K. H. Nagai, Y. Shitaka, D. Tanaka, K. Yoshikawa, H. Chaté, and K. Oiwa, Nature (London) **483**, 448 (2012).
[8] A. Bricard, J.-B. Caussin, N. Desreumaux, O. Dauchot, and D. Bartolo, Nature (London) **503**, 95 (2013).
[9] M. C. Marchetti, J. F. Joanny, S. Ramaswamy, T. B. Liverpool, J. Prost, M. Rao, and R. A. Simha, Rev. Mod. Phys. **85**, 1143 (2013).
[10] S. Ramaswamy, Annu. Rev. Condens. Matter Phys. **1**, 323 (2010).
[11] A. P. Solon, H. Chaté, and J. Tailleur, Phys. Rev. Lett. **114**, 068101 (2015).
[12] G. Grégoire and H. Chaté, Phys. Rev. Lett. **92**, 025702 (2004).
[13] J. Toner and Y. Tu, Phys. Rev. Lett. **75**, 4326 (1995).
[14] J. Toner, Y. Tu, and S. Ramaswamy, Ann. Phys. (Amsterdam) **318**, 170 (2005).
[15] A. Attanasi, A. Cavagna, L. D. Castello, I. Giardina, T. S. Grigera, A. Jelić, S. Melillo, L. Parisi, O. Pohl, E. Shen *et al.*, Nat. Phys. **10**, 691 (2014).
[16] A. Cavagna, L. D. Castello, I. Giardina, T. Grigera, A. Jelic, S. Melillo, T. Mora, L. Parisi, E. Silvestri, M. Viale *et al.*, J. Stat. Phys. **158**, 601 (2015).
[17] A. Cavagna, I. Giardina, T. S. Grigera, A. Jelic, D. Levine, S. Ramaswamy, and M. Viale, Phys. Rev. Lett. **114**, 218101 (2015).
[18] F. D. C. Farrell, M. C. Marchetti, D. Marenduzzo, and J. Tailleur, Phys. Rev. Lett. **108**, 248101 (2012).
[19] D. S. Dean, J. Phys. A **29**, L613 (1996).
[20] R. Zwanzig, *Nonequilibrium Statistical Mechanics* (Oxford University Press, New York, 2001).
[21] H. Risken, *The Fokker-Planck Equation*, 2nd ed., (Springer-Verlag, Berlin, 1988).
[22] E. Bertin, M. Droz, and G. Grégoire, J. Phys. A **42**, 445001 (2009).
[23] A. Peshkov, E. Bertin, F. Ginelli, and H. Chaté, Eur. Phys. J. Spec. Top. **223**, 1315 (2014).
[24] See Supplemental Material http://link.aps.org/supplemental/10.1103/PhysRevLett.115.258101 at for a description of our choice of parameters.
[25] S. Mishra, A. Baskaran, and M. C. Marchetti, Phys. Rev. E **81**, 061916 (2010).
[26] J. C. Tsai, F. Ye, J. Rodriguez, J. P. Gollub, and T. C. Lubensky, Phys. Rev. Lett. **94**, 214301 (2005).
[27] E. Braun, O. L. Fuchs, and S. Godoy, Chem. Phys. Lett. **265**, 434 (1997).
[28] J. T. Hynes, R. Kapral, and M. Weinberg, Physica (Amsterdam) **87A**, 427 (1977).
[29] E. Bertin, M. Droz, and G. Grégoire, Phys. Rev. E **74**, 022101 (2006).